JACS
JOURNAL OF THE AMERICAN CHEMICAL SOCIETY
Article
pubs.acs.org/JACS

Enhancing the Photocurrent in Diketopyrrolopyrrole-Based Polymer Solar Cells via Energy Level Control

Weiwei Li, W. S. Christian Roelofs, Martijn M. Wienk, and René A. J. Janssen*

Molecular Materials and Nanosystems, Eindhoven University of Technology, P.O. Box 513, 5600 MB Eindhoven, The Netherlands

Supporting Information

ABSTRACT: A series of diketopyrrolopyrrole (DPP)-based small band gap polymers has been designed and synthesized by Suzuki or Stille polymerization for use in polymer solar cells. The new polymers contain extended aromatic π-conjugated segments alternating with the DPP units and are designed to increase the free energy for charge generation to overcome current limitations in photocurrent generation of DPP-based polymers. In optimized solar cells with [6,6]phenyl-C_{71}-butyric acid methyl ester ([70]PCBM) as acceptor, the new DPP-polymers provide significantly enhanced external and internal quantum efficiencies for conversion of photons into collected electrons. This provides short-circuit current densities in excess of 16 mA cm^{-2}, higher than obtained so far, with power conversion efficiencies of 5.8% in simulated solar light. We analyze external and internal photon to collected electron quantum efficiencies for the new polymers as a function of the photon energy loss, defined as the offset between optical band gap and open circuit voltage, and compare the results to those of some of the best DPP-based polymers solar cells reported in the literature. We find that for the best solar cells there is an empirical relation between quantum efficiency and photon energy loss that presently limits the power conversion efficiency in these devices.

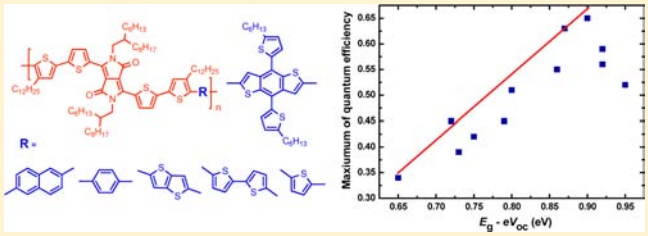

1. INTRODUCTION

Polymers solar cells based on conjugated polymers as electron-donor material and fullerene (C_{60} or C_{70}) derivatives as acceptor form an attractive approach for future renewable energy production because they combine high power conversion efficiencies (PCEs) up to 8% with flexibility and low cost.[1,2] A myriad of semiconducting conjugated polymers has been designed in recent years to achieve high photocurrents, open circuit voltage, and performance.[3−17] Among these materials numerous small band gap polymers that feature a broad absorption, extending into the near-infrared (near-IR) region, have been synthesized by alternating electron-rich and electron-deficient units along the polymer chain. To further enhance the power conversion efficiencies of polymer solar cells, new materials are required. This especially holds for polymer tandem solar cells, where photoactive layers with wide and small optical band gaps are combined to enhance absorption of light and minimize the loss of photon energies. Polymer tandem cells already provide PCEs higher than those of the corresponding single junctions[18,19] but are still significantly below the anticipated maximum-reachable performance.[20] Besides improvement of the recombination layers and interface with electrodes, new small band gap materials are needed to reduce energy losses and increase photocurrent density.

In designing new polymers for organic solar cells many parameters must be considered, such as optical band gap, absorption coefficient, oxidation and reduction potentials, charge carrier mobility, molecular weight, morphology, crystallinity, solubility, and ease and reproducibility of synthesis. Detailed design rules that comprise all of these are presently unknown. However, it is well established that the highest occupied molecular orbital (HOMO) of the polymer and lowest unoccupied molecular orbital (LUMO) levels of the fullerene derivative determine the open circuit voltage (V_{oc}).[21] The short circuit current density (J_{sc}) is principally limited by the number of absorbed photons and, hence, by the optical band gaps of both donor and acceptor. As a consequence of the principal trade-off between V_{oc} and J_{sc}, optimization of the PCE is not trivial.

Conjugated polymers that incorporate diketopyrrolopyrrole units (DPP) are attracting interest for application in ambipolar field effect transistors and organic solar cells in recent years.[22−24] Because of their property to self-organize, DPP-based polymers feature high charge carrier mobilities. Furthermore, the electron-deficient nature of the DPP unit provides the possibility to control the optical band gap into the near-IR region of the spectrum via copolymerization with electron-rich aromatic heterocycles or conjugated oligomers with electron-donating properties. Currently the best DPP-based polymer solar cells give a PCE of 6.5% when combined with [6,6]phenyl-C_{71}-butyric acid methyl ester ([70]PCBM) as acceptor.[19] However, in all DPP-based polymers published to date, the J_{sc} is less than expected, due to a limited quantum efficiency for converting incident photons to electrons. The

Received: June 3, 2012
Published: July 20, 2012

   dx.doi.org/10.1021/ja305358z | J. Am. Chem. Soc. 2012, 134, 13787−13795

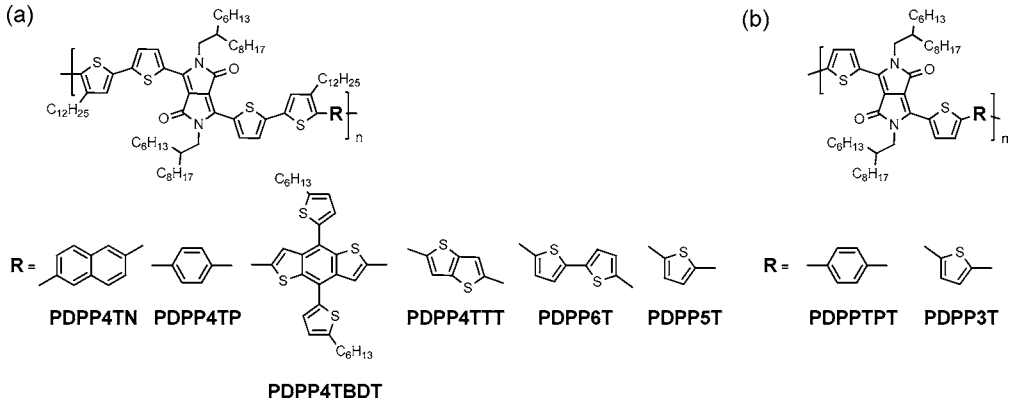

Figure 1. (a) DPP-based conjugated polymers described in this work. (b) PDPPTPT and PDPP3T described in refs 24 and 27.

Scheme 1. Synthesis Route of DPP-Based Monomer and Polymers[a]

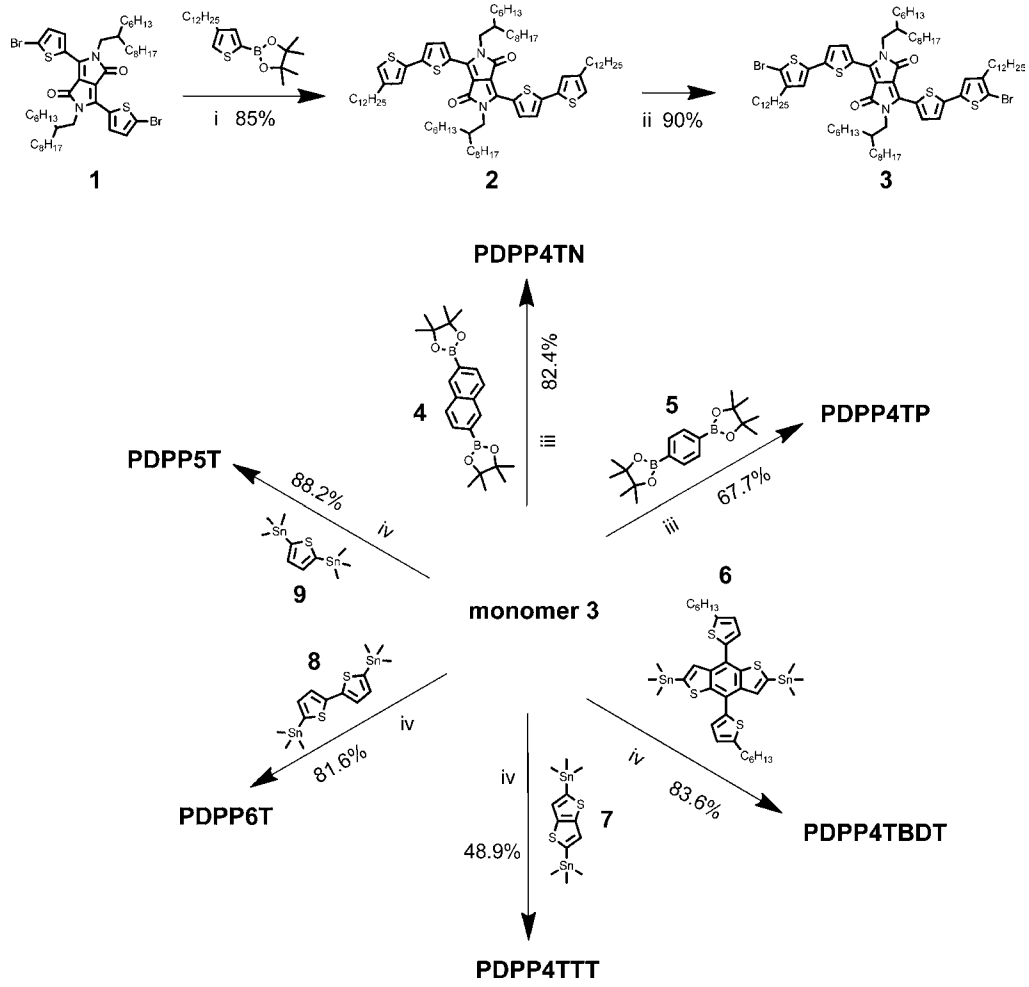

[a]Reaction conditions: (i) $Pd(PPh_3)_4/K_2CO_3$ (aq)/Aliquat 336 in toluene at 115 °C; (ii) NBS in $CHCl_3$ at 0 °C; (iii) Suzuki polymerization to PDPP4TN and PDPP4TP using $Pd_2(dba)_3/[(t\text{-}Bu)_3PH]BF_4/K_3PO_4$ (aq) in THF at 80 °C; and (iv) Stille polymerization to PDPP4TBDT, PDPP4TTT, PDPP5T, and PDPP6T using $Pd_2(dba)_3/PPh_3$ in toluene/DMF (5:1, v/v) at 115 °C.

highest external quantum efficiencies (EQEs) for DPP-based solar cells are ~50%,[25] but often significantly less. The limited EQE may originate from a low absorption coefficient or from a low internal quantum efficiency (IQE), i.e., a poor conversion of absorbed photons in the collected charges. Presently the factors that influence the magnitude of the IQE are not fully understood.[26] For PDPPTPT (Figure 1) we identified that recombination of photogenerated charges into the triplet state of the polymer occurs in blends with [70]PCBM and limits the EQE.[27] The triplet formation is a consequence of the poor tendency for spatial separation of photogenerated charges which causes geminate recombination into a triplet state. In PDPPTPT:[70]PCBM layers, charge generation is less a problem than charge separation. For small band gap polymers,

dx.doi.org/10.1021/ja305358z | J. Am. Chem. Soc. 2012, 134, 13787−13795

Table 1. Molecular Weight and Optical Properties of the DPP Polymers

				$CHCl_3$ solution			film		
polymer	M_n[a] (kg mol^{-1})	M_w[a] (kg mol^{-1})	PDI	λ_{peak} (nm)	λ_{onset} (nm)	E_g^{sol} (eV)	λ_{peak} (nm)	λ_{onset} (nm)	E_g^{film} (eV)
PDPP4TN	12.1	37.6	3.11	628	738	1.68	633, 689	764	1.62
PDPP4TP	32.4	87.3	2.69	628	742	1.67	636, 697	806	1.54
PDPP4TBDT	41.8	126.5	3.03	666	821	1.51	677, 722	832	1.49
PDPP4TTT	22.8	68.4	3.0	668	821	1.51	698, 743	835	1.48
PDPP6T	37.9	111.8	2.95	665	816	1.52	695, 744	835	1.48
PDPP5T	36.8	111.5	3.03	677	805	1.54	698, 758	849	1.46
PDPPTPT[b]	–	–	–	748	794	1.56	692, 761	811	1.53
PDPP3T[c,d]	54.0	170.1	3.15	826	912	1.36	769, 849	954	1.30

[a]Determined with GPC at 80 °C using *o*-DCB as the eluent. [b]Ref 27. [c]Ref 24. [d]Solution data in *o*-DCB.

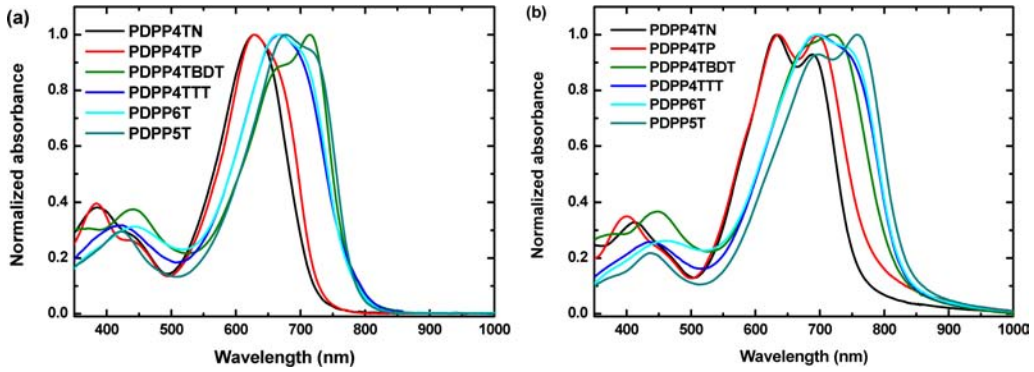

Figure 2. Electronic absorption spectra of the DPP polymers (a) in $CHCl_3$ solution and (b) in solid state films.

especially for those with optical absorption extending to 900 nm and beyond, as required for tandem solar cells, the energy offset between the LUMO levels of the polymer and fullerene is reduced, which likely contributes to the decreased photocurrent.[28−31] Considering the LUMO offset, it has been argued that the efficiency of charge separation is controlled by the free energy for charge generation,[32−34] and there is little doubt that the electron and hole formed in the photoinduced charge-transfer reaction use some of their initial excess energy (with respect to a fully relaxed charge-transfer state) to overcome their Coulomb binding energy in separating from the donor−acceptor interface. An important question, however, is how large the required excess energy really is. This has been a subject of several recent studies, from which a consistent picture is still difficult to discern.[35−38]

In this work we focus on designing and synthesizing new DPP-based conjugated polymers with energy levels that enable significantly higher EQEs and attempt to understand the effect of the free energy for charge generation on current density and quantum efficiency. The new DPP-polymers consist of a common bis(dithiophene)-DPP unit alternating with a variety of different aromatic units. Compared to most existing DPP-polymers, the new materials feature an extended π-conjugated electron-rich segment. This increases the HOMO and LUMO levels in the polymer because of the larger content of electron-rich aromatic units and the less and more isolated electron-deficient units. By virtue of this shift, the free energy for charge generation will increase albeit at the cost of a lower V_{oc}. We demonstrate that this strategy is a viable method to increase the quantum efficiency for charge generation and provides significantly higher photocurrent densities up to 16 mA cm^{-2} and power conversion efficiencies approaching 6%. We analyze the internal and external quantum efficiencies of the new materials as function of the free energy for charge generation and compare them with those reported for other DPP polymers to identify the origin of intrinsic limitation in solar energy conversion in these materials.

2. RESULTS AND DISCUSSION

2.1. Synthesis. The synthesis of the monomers and polymers is shown in Scheme 1. The key DPP monomer **3** was synthesized by Suzuki reaction of 3,6-bis(5-bromo-2-thienyl)-2,5-dihydro-2,5-di(2′-hexyldecyl)-pyrrolo[3,4c]-pyrrolo-1,4-dione (**1**) with 2-(4-dodecylthiophen-2-yl)-4,4,5,5-tetramethyl-1,3,2-dioxaborolane to yield **2** and subsequent bromination with NBS in an overall yield of 76.5%. The dodecyl side chains are introduced to improve the solubility and to tailor the energy level in this monomer. The conjugated polymers shown in Scheme 1 have been prepared using Suzuki and Stille polymerization. Particular attention was given to optimize the reaction conditions to achieve high molecular weight because this is one of key factors controlling the device performance. As an example, PDPP4TP synthesized in a Suzuki reaction of **3** with 1,4-bis(4,4,5,5-tetramethyl-1,3-dioxaboralane)benzene affords a high molecular weight of M_n = 32.4 kg mol^{-1} when using $Pd_2(dba)_3$ as a catalyst with $[(t\text{-}Bu)_3PH]BF_4$ as ligand in $THF/H_2O/K_3PO_4$. Under these conditions, the reactivity is high and the molecular weight is greatly improved compared to the traditional $Pd_2(dba)_3/PPh_3$ catalyst/ligand system in toluene/H_2O/K_3PO_4 which provides a much lower molecular weight of M_n = 6.5 kg mol^{-1}. The same polymerization method was used for PDPP4TN, which incorporates a naphthalene unit, to afford a molecular weight of M_n = 12.1 kg mol^{-1}. PDPP4TBDT, PDPP5T, and PDPP6T were readily obtained by Stille polymerization in toluene/DMF in high yields and molecular weights (Scheme 1 and Table 1; the GPC data are provided in the Supporting Information,

dx.doi.org/10.1021/ja305358z | J. Am. Chem. Soc. 2012, 134, 13787−13795

Figure S1). For PDPP4TTT the molecular weight of the isolated fraction was somewhat less because the high molecular weight fraction is insoluble in chloroform. After optimization of the reaction conditions, the DPP polymers were obtained in similarly high molecular weights (Table 1). This is advantageous for achieving high photovoltaic performance and convenient for direct comparison of the polymers.

2.2. Optical and Electrochemical Properties. The strong electron-withdrawing character of the DPP unit efficiently shifts the electronic absorption of the DPP polymers to the near-IR region. The DPP polymers exhibit relatively broad spectra with absorption onsets ranging from 740 to 820 nm in chloroform solution, as shown in Figure 2a and Table 1. The absorption of the polymers that incorporate naphthalene and phenylene as comonomer is blue-shifted compared to those that have a thiophene-based comonomer. This is a result of the combination of a less electron-donating character and of steric hindrance for planarization which reduces the conjugation along the polymer chain. In the solid-state films, the electronic absorption shifts bathochromically as a result of aggregation. The onsets of absorption now range from 770 to 850 nm (Figure 2 and Table 1). The new PDPP4TP and PDPP5T polymers that have two additional dodecylthiophene units show the expected blue shift of the electronic absorption with respect to the previously reported polymers PDPPTPT and PDPP3T. Figure 2 and Table 1 show that PDPP5T has the most pronounced red shift in the solid state versus solution compared to the other polymers, resulting in the lowest optical band gap of 1.46 eV in films. The aggregation phenomenon is supported by the pronounced shoulder peak at high wavelength in films.

Cyclic voltammetry (Supporting Information, Figure S2) was performed for DPP polymers dissolved in *o*-DCB, and the results are summarized at Table 2. As expected the extended π-conjugated electron-rich segment of the new DPP polymers decreases the redox potentials (i.e., higher HOMO and LUMO levels) compared to those with a shorter repeating unit (Table 2) because of a higher number of electron-rich aromatic units and less and more isolated electron-deficient units. The electrochemical band gap was determined as the difference between the onsets of the oxidation and reduction waves ($E_g^{CV} = e(E_{ox} - E_{red})$). E_g^{CV} follows the same trend as E_g^{sol} (Table 2) but is larger by 0.05−0.25 eV. The reduction potential E_{red} of the new DPP polymers is more negative than those of PDPPTPT and PDPP3T. As a consequence, the offset α between the LUMO levels of the new DPP polymers and [70]PCBM is 0.58−0.65 V and significantly higher than that the corresponding offsets for PDPPTPT (0.50 V) and PDPP3T (0.42 V) (Table 2). Empirically, it has been found that a LUMO offset α between polymer and fullerene should be at least 0.3 V for the efficient exciton dissociation into charge carriers [39] and that higher offsets enhance the driving force for charge generation and improve photocurrent in bulk heterojunction photovoltaic devices.[40] The oxidation potentials E_{ox} of the new polymers are lower than that of PDPPTPT and PDPP3T, and this increase in HOMO level energy is expected to result in a concomitant loss in V_{oc} when the polymers are combined with a common fullerene acceptor.

Table 2. Electrochemical Properties and LUMO Offset of the DPP Polymers

polymer	E_{red} (V)[a]	E_{ox} (V)[a]	E_g^{CV} (eV)	α (V)[b]
PDPP4TN	−1.69	0.05	1.74	0.62
PDPP4TP	−1.70	0.04	1.74	0.63
PDPP4TBDT	−1.66	−0.02	1.64	0.59
PDPP4TTT	−1.65	0.06	1.71	0.58
PDPP6T	−1.68	−0.02	1.66	0.61
PDPP5T	−1.72	0.07	1.65	0.65
PDPPTPT[c]	−1.57	0.25	1.82	0.50
PDPP3T[d]	−1.49	0.07	1.56	0.42

[a]Versus Fc/Fc^+. [b]$\alpha = E_{red}([70]PCBM) - E_{red}$, with $E_{red}([70]PCBM) = -1.07$ vs Fc/Fc^+.[41] [c]Ref 27. [d]Ref 24.

2.3. Charge Carrier Mobility. The charge carrier mobility of the conjugated polymers is important for their performance photovoltaic cells. A high mobility facilitates charge separation from the donor−acceptor interface and charge transport to the electrodes and reduces recombination. The mobility of the polymers was determined in a field-effect transistor (FET) configuration. The FETs were fabricated in a bottom gate − bottom contact configuration. The silicon dioxide gate dielectric used was passivated with hexamethyldisilazane (HMDS), and gold source and drain electrodes were defined using conventional photolithography. The polymers were applied via spin coating from $CHCl_3$ solution and thermally annealed for 24 h at 200 °C in vacuum. The DPP polymers exhibit ambipolar transfer characteristics (Figure 3) indicating their ability to transport both holes and electrons. The hole mobility, μ_h, of the DPP polymers exceeds 10^{-2} cm^2 V^{-1} s^{-1} and is similar to those of PDPPTPT and PDPP3T,[24,27] except for PDPP4TN and PDPP4TBDT where $\mu_h \approx 10^{-3}$ cm^2 V^{-1} s^{-1} (Table 3). The electron mobility, μ_e, of the new DPP polymers is consistently 1 order of magnitude lower than μ_h (Table 3). Such a strong difference between μ_h and μ_e was not found for PDPP3T and PDPPTPT (Table 3).[24,27] The difference likely originates from the higher LUMO levels of the new DPP polymers. A higher LUMO level is unfavorable for electron transport in FETs because it reduces electron injection from the gold electrodes and enhances the probability for electron trapping at the SiO_2 surface.

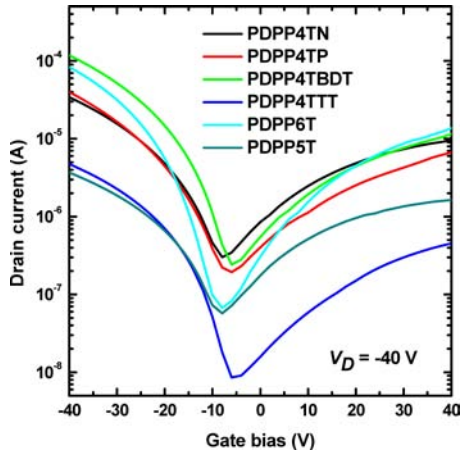

Figure 3. Ambipolar transfer characteristics for FETs for the DPP polymers recorded at a drain bias of $V_D = -40$ V. The length and width of the transistor are 40 μm and 10 mm, respectively.

2.4. Photovoltaic Properties. Photovoltaic cells were made by sandwiching blends of the DPP polymers as electron donor with [70]PCBM as electron acceptor between an ITO/PEDOT:PSS front electrode and a LiF/Al back electrode. The

dx.doi.org/10.1021/ja305358z | J. Am. Chem. Soc. 2012, 134, 13787−13795

Table 3. Field Effect Hole and Electron Mobility of the DPP Polymers

polymer	μ_h ($cm^2\ V^{-1}\ s^{-1}$)	μ_e ($cm^2\ V^{-1}\ s^{-1}$)
PDPP4TN	1.5×10^{-3}	1.0×10^{-4}
PDPP4TP	3.5×10^{-2}	5.0×10^{-3}
PDPP4TBDT	1.0×10^{-3}	3.0×10^{-4}
PDPP4TTT	2.0×10^{-2}	1.0×10^{-3}
PDPP6T	5.0×10^{-2}	3.0×10^{-3}
PDPP5T	1.5×10^{-2}	1.5×10^{-3}
PDPPTPT	4.0×10^{-2}	2.0×10^{-2}
PDPP3T	4.0×10^{-2}	1.0×10^{-2}

active layers were applied by spin coating, and the deposition was optimized for the blend ratio, the layer thickness, and the processing additive (or cosolvent). All DPP polymers gave the best photovoltaic performance when blended with [70]PCBM in a 1:2 ratio by weight with [70]PCBM and an active layer thickness around 90 nm. However, the optimal processing additive used in combination with $CHCl_3$ as spin coating solvent is quite different for the different DPP polymers (Table 4). The current density−voltage (J−V) characteristics of the optimized cells in the dark and under illumination are shown in Figure 4a and corresponding performance parameters are collected in Table 4 and compared with those of PDPPTPT and PDPP3T. As expected the new DPP polymers give lower V_{oc} than that of PDPPTPT or PDPP3T due to their lower oxidation potential, but their current density is consistently enhanced, with the highest current density of 16.4 mA cm^{-2} reached for PDPP5T. The optimized photoactive layers exhibit a rather smooth surface with an rms roughness of 1.2−2.6 nm, indicating a well-mixed morphology that enhances exciton dissociation and charge generation (see Supporting Information, Figure S3). The increased current density obtained for the new DPP polymers is also reflected in an improved EQE, as shown in Figure 4b. While the EQE of PDPPTPT and PDPP3T maximize at ∼0.39 and ∼0.34,[24,27] the maximum EQE for the new DPP polymers increases to around 0.6 in the region where the polymer absorbs and is the highest at 0.65 for PDPP5T. It is important to note that also in the spectral range of 400−550 nm, where there is a strong contribution from [70]PCBM to the absorption of light, the EQE remains high. The new DPP polymers generally afford a high fill factor (FF) in blends with [70]PCBM, taking advantage of the high hole mobility. As a result of the combined effects, the new DPP polymers afford a PCE in the range of 4.5−5.8%. Among these polymers, PDPP5T that has a quinquethiophene donor unit alternating with DPP gave the best PCE of 5.8%.

2.5. Internal Quantum Efficiency and Photon Energy Loss. To better understand the origin of the increased current density in the DPP polymers, we determined the IQE for these devices. To this end, we first determine the wavelength-dependent refractive index $n(\lambda)$ and extinction coefficient $k(\lambda)$ of the photoactive layers (see Supporting Information, Figure S4). We use this data to calculate the fraction of photons absorbed in the photoactive layer via optical modeling using a transfer matrix formalism, which involves the complex refractive index and thickness of all materials in the device as input. Figure 5a reveals that the calculated fraction of photons absorbed from the incident light is about 80% for all DPP-polymer:[70]PCBM films at the optimized layer thickness (in the range of 90−110 nm). The shape of the curves is similar to the EQE shown in Figure 4b. Mutual deviations are small for the DPP-polymers that have the same optical band gap. The only significant deviation is observed for the PDPP4TBDT:[70]PCBM blend, which absorbs about 10% less photons in the entire spectral range. This difference possibly originates from the two thiophene units on the BDT unit, which gives a low contribution to the absorption in the near-IR region but do of course contribute to the thickness.

Figure 5b shows the IQE calculated from the EQE and the fraction of photons absorbed in the photoactive layer for the DPP-polymers:[70]PCBM photoactive layers and for of PDPPTPT:[70]PCBM and PDPP3T:[70]PCBM reported previously.[24,27] The shapes of the IQE curves are rather flat, although they tend to roll off at the highest wavelengths. The IQEs of the new DPP-polymers with [70]PCBM are higher than those of PDPPTPT and PDPP3T, except for PDPP4TN which has a significantly lower molecular weight leading to less effective optimized morphology.[16,24] The lower IQE of PDPPTPT and PDPP3T compared to new DPP-polymers coincides with the smaller offset α between the LUMO level of the polymer and the LUMO of [70]PCBM (Table 4).

It is important to note that the molecular weight of the donor polymers can have a substantial effect on the performance of polymer solar cells.[16,24,42] For PDPP4TP we confirm this dependence in the Supporting Information (Figure S5, Table S1). This complicates establishing structure−property relationships. We note, however, that for most polymers in this study M_n exceeds 30 kg mol^{-1} (Table 1), where the effects of molecular weight on performance generally seem to saturate.[16,24,42]

Another way to analyze the IQE and EQE for the different DPP-polymers is by comparing them to the total photon energy loss in the device. The total photon energy loss can be defined as $E_g - eV_{oc}$, where E_g is the optical band gap of the blend. In Figure 6a we compare the solar spectrum (AM1.5G)

Table 4. Characteristics of Optimized Solar Cells of the DPP Polymers with [70]PCBM

polymer	solvent	thickness (nm)	J_{sc}[a] (mA cm^{-2})	V_{oc} (V)	FF	PCE[a] (%)	EQE$_{max}$[b]	IQE	$E_g - eV_{oc}$ (V)
PDPP4TN	$CHCl_3$:*o*-DCB 10%	98	10.3	0.67	0.66	4.5	0.52	0.59	0.95
PDPP4TP	$CHCl_3$:*o*-DCB 10%	86	12.0	0.67	0.69	5.5	0.63	0.68	0.87
PDPP4TBDT	$CHCl_3$:DIO 2.5%	113	13.9	0.63	0.55	4.8	0.55	0.73	0.86
PDPP4TTT	$CHCl_3$:*o*-DCB 10%	104	14.8	0.56	0.62	5.1	0.59	0.68	0.92
PDPP6T	$CHCl_3$:DIO 2.5%	111	14.3	0.56	0.65	5.2	0.56	0.64	0.92
PDPP5T	$CHCl_3$:*o*-DCB 5%	110	16.4	0.56	0.64	5.8	0.65	0.72	0.90
PDPPTPT[c]	$CHCl_3$:DIO 1.4%	90	10.8	0.80	0.65	5.5	0.39	0.54	0.73
PDPP3T[d]	$CHCl_3$:DIO 5.5%	90	11.8	0.65	0.60	4.7	0.34	0.49	0.65

[a] J_{sc} was calculated by integrating the EQE spectrum with the AM1.5G spectrum. [b] Measured in the region of polymer absorption. [c] Ref 27. [d] Ref 24.

dx.doi.org/10.1021/ja305358z | J. Am. Chem. Soc. 2012, 134, 13787−13795

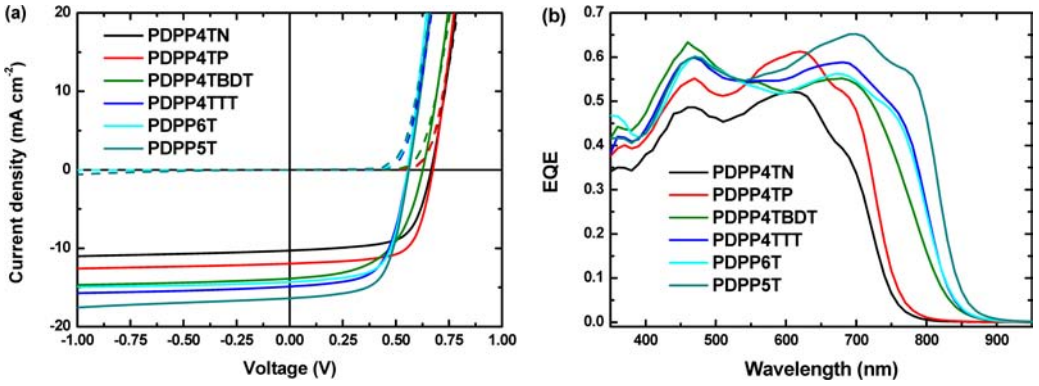

Figure 4. (a) J–V characteristics in dark (dashed lines) and under white light illumination (solid lines) of optimized solar cells of the DPP polymers with [70]PCBM. (b) EQE of the same devices.

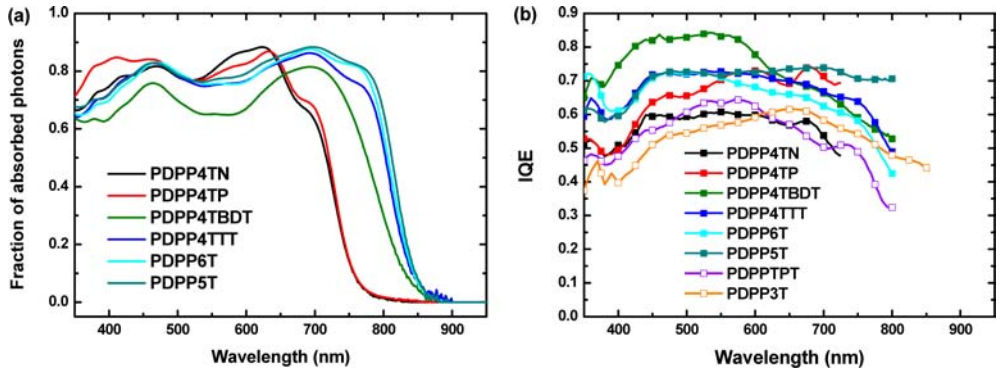

Figure 5. (a) Fraction of photons absorbed in the photoactive layers for DPP-polymer:[70]PCBM films. (b) IQE DPP-polymer:[70]PCBM films.

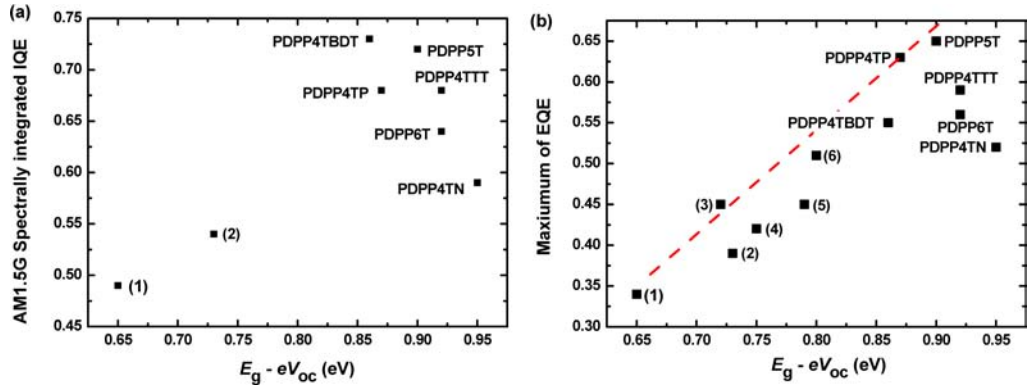

Figure 6. (a) AM1.5G spectrally integrated IQE versus to photon energy loss in the device. (b) Maximum EQE from polymer absorption region related to photo energy loss. Data from literature are: (1) PDPP3T:[70]PCBM, PCE = 4.7%, ref 24; (2) PDPPTPT:[70]PCBM, PCE = 5.5%, ref 27, (3) PBDTT-DPP:[70]PCBM, PCE = 6.5%, ref 19, (4) PDPP2FT-C14:[70]PCBM, PCE = 6.2%, ref 43; (5) PBBTDPP2:[70]PCBM, PCE = 4.0%, ref 23; and (6) P1:[70]PCBM, PCE = 5.4%, ref 25.

spectrally integrated IQE versus $E_g - eV_{oc}$ for the different photoactive layers. The AM1.5G spectrally integrated IQE is obtained by taking the ratio of the EQE integrated over the solar spectrum (representing J_{sc}) with the total number of photons absorbed obtained from integrating the fraction of absorbed photons over the solar spectrum. The photon energy loss can be considered as the loss in free energy in converting band edge photons at to collectable charge carriers at open circuit. Of course $E_g - eV_{oc}$ is related to the offset between the LUMO levels α (provided that it less than the offset between the HOMO levels), but it has the important advantage that it can be determined more accurately and from the actual device. It has previously been argued that $E_g - eV_{oc} \geq 0.6$ V for organic solar cells.[33] Figure 6a shows that the new DPP-polymers provide higher integrated IQEs than PDPPTPT and PDPP3T[24,27] but at the cost of a larger photon energy loss. The highest values are over 70% for PDPP4TBTD and PDPP5T. This suggests that an increased photon energy loss results in a higher quantum yield. For some of the new materials, Figure 6a shows in fact an opposite trend. We stress, however, that likely many more materials can be found with a low IQE, irrespective of the $E_g - eV_{oc}$ value, because of other important factors, such as suboptimal morphology (often found for lower molecular weights), and low charge carrier mobility can also limit the IQE. The significant result in Figure 6a is that there are no data points in the upper left corner.

dx.doi.org/10.1021/ja305358z | J. Am. Chem. Soc. 2012, 134, 13787–13795

Of course it can be argued that the PDPPTPT and PDPP3T, described by us previously, form only a small, and hence possibly unrepresentative, subset of materials. Therefore we compare in Figure 6b for some of the most efficient DPP-polymers published to date, the maximum in the EQE to the photon energy loss. The maximum in the EQE is a less relevant parameter than the spectrally integrated IQE, but the latter values have not been reported. Figure 6b confirms the trend observed in Figure 6a in the sense that a higher photon energy loss coincides with a higher EQE. In considering Figure 6b we emphasize again that it is not expected that there is a simple relation between IQE and $E_g - eV_{oc}$, because collection of charges involves many more parameters (e.g., charge carrier mobility) than the ones that determine the energy. Nevertheless one could argue that in the best photoactive layers, charge collection is close to optimal. The red dashed line in Figure 6b can be considered as a measure of the best of what has been achieved in terms of compromising EQE and $E_g - eV_{oc}$. The truly optimal material of course would combine a small $E_g - eV_{oc}$ with a high EQE. So far no materials that represent a data point in the upper left part of the Figure 6a are known.

From these results we are inclined to conclude that the increased photon energy loss, defined as $E_g - eV_{oc}$, is an important parameter in enhancing exciton dissociation and charge separation. For the new DPP-polymers developed in this work such correlation is hampered by the small (~100 meV) difference in $E_g - eV_{oc}$ among the materials, which makes that differences in charge carrier mobility, active layer morphology, and also possibly interface issues may obscure the EQE data. But comparing to other materials, such relation seems to be present for these DPP-polymers.

Although our experimental results clearly point to a relation of EQE and IQE with $E_g - eV_{oc}$ it should be noted that there is quite some experimental and theoretical evidence which suggests that the loss in free energy is not an decisive factor in charge separation.[35,37,44−46] Compelling experimental evidence for the absence of such relation, at least in the materials studied, is the fact that the IQE has been found to be independent of the excitation wavelength, even when comparing excitation above the optical band gap ($h\nu > E_g$) and in the charge-transfer band ($E_{CT} < h\nu < E_g$).[44] Likewise the electric field dependence of charge generation has been found to be small for sub gap, i.e., $E_{CT} < h\nu < E_g$, excitation in selected examples.[36,38] We note that since $E_{CT} \approx eV_{oc}$ + 0.5 eV, the energy of E_{CT} remains substantially above eV_{oc}.

3. CONCLUSIONS

A series of new DPP-polymers with extended electron-rich π-conjugated segments has been synthesized via Suzuki and Stille reactions. The new DPP-polymers feature small optical band gaps, high molecular weight, high charge carrier mobility, and sufficient free energy for charge generation to [70]PCBM as an acceptor. As a consequence, the DPP-polymers afford high current densities and fill factors and hence give power conversion efficiency up to 5.8% in bulk heterojunction solar cells. The external and internal quantum efficiencies for photon to collected electron conversion of 65% and 70%, obtained for photons absorbed by the polymer, are significantly higher than obtained for other DPP-polymers described to date. We demonstrate an empirical relation between the photon energy loss, defined as $E_g - eV_{oc}$, and the maximum photon to collected electron quantum efficiency for DPP-polymers (Figure 6) that presently limits the power conversion efficiency of these solar cells. Future research will focus on understanding the detailed origin of this relation and designing materials that allow approaching the intrinsic limitations more closely.

4. EXPERIMENTAL SECTION

4.1. Materials and Measurement. All synthetic procedures were performed under argon atmosphere. Commercial chemicals were used as received. Dry solvents were distilled over 4 Å molecular sieves. [70]PCBM (purity ~95%) was purchased from Solenne BV. 3,6-Bis(5-bromo-2-thienyl)-2,5-dihydro-2,5-di(2′-hexyldecyl)-pyrrolo-[3,4c]pyrrolo-1,4-dione (**1**),[23] 2-(4-dodecylthiophen-2-yl)-4,4,5,5-tetramethyl-1,3,2-dioxaborolane,[47] 2,2′-(2,6-naphthalenediyl)bis[4,4,5,5-tetramethyl-1,3,2-dioxaborolane (**4**),[48] 2,6-bis(trimethyltin)-4,8-bis(5-hexylthiophene-2-yl)benzo[1,2-*b*:4,5-*b*′]dithiophene (**6**),[49] 2,5-bis-(trimethylstannyl)thieno[3,2-b]thiophene (**7**),[50] and 5,5′-bis-(trimethylstannyl)-2,2′-bithiophene (**8**)[51] were synthesized according to literature procedures.

^{1}H NMR and ^{13}C NMR spectra were recorded at 400 and 100 MHz on a VARIAN mercury spectrometer with $CDCl_3$ as the solvent and tetramethylsilane (TMS) as the internal standard. Molecular weight was determined with GPC at 80 °C on a PL-GPC 120 system using a PL-GEL 5u MIXED-C column and *o*-DCB as the eluent and against polystyrene standards. Electronic spectra were recorded on a Perkin-Elmer Lambda 900 UV−vis near-IR spectrophotometer. Cyclic voltammetry was conducted with a scan rate of 0.1 V s^{-1} under an inert atmosphere with 1 M tetrabutylammonium hexafluorophosphate in *o*-DCB as the electrolyte. The working electrode was a platinum disk, and the counter electrode was a silver electrode. The concentration of the sample in the electrolyte was approximately 1 mM, based on monomers. Fc/Fc$^+$ was used as an internal standard.

Field-effect transistors were fabricated using heavily doped silicon wafers as the common gate electrode with a 200 nm thermally oxidized SiO_2 layer as the gate dielectric. Using conventional photolithography, gold source and drain electrodes were defined in a bottom contact device configuration with a channel width and length of 2500 and 10 μm, respectively. A 10 nm layer of titanium was used, acting as an adhesion layer for the gold on SiO_2. The SiO_2 layer was exposed to the vapor of the primer hexamethyldisilazane for 60 min prior to semiconductor deposition in order to passivate the surface of the dielectric. Polymer films were spun from a chloroform solution (4 mg/mL) at 1500 rpm for 30 s. Freshly prepared devices were annealed in a dynamic vacuum of 10^{-5} mbar at 200 °C for 24 h to remove traces of the solvent. All electrical measurements were performed in vacuum using an HP 4155C semiconductor parameter analyzer.

Photovoltaic devices were made by spin coating poly-(ethylenedioxythiophene):poly(styrene sulfonate) (PEDOT:PSS) (Clevios P, VP AI 4083) onto precleaned, patterned indium tin oxide (ITO) substrates (14 Ω per square) (Naranjo Substrates). The photoactive layer was deposited by spin coating a chloroform solution containing the polymers and [70]PCBM with 1:2 (w/w) ratio and the appropriate amount of 1,8-diiodooctane (DIO) or *o*-DCB. LiF (1 nm) and Al (100 nm) were deposited by vacuum evaporation at ~2×10^{-7} mbar as the back electrode. The active area of the cells was 0.091 or 0.162 cm^2, and no size dependence was found between these two dimensions. *J*−*V* characteristics were measured under ~100 mW cm^{-2} white light from a tungsten-halogen lamp filtered by a Schott GG385 UV filter and a Hoya LB 120 daylight filter, using a Keithley 2400 source meter. Short circuit currents under AM1.5G conditions were estimated from the spectral response and convolution with the solar spectrum. The spectral response was measured under simulated 1 sun operation conditions using bias light from a 532 nm solid-state laser (Edmund Optics). Light from a 50 W tungsten halogen lamp (Osram64610) was used as probe light and modulated with a mechanical chopper before passing the monochromator (Oriel, Cornerstone 130) to select the wavelength. The response was recorded as the voltage over a 50 resistance, using a lock-in amplifier (Stanford Research Systems SR 830). A calibrated Si cell was used as reference. The device was kept behind a quartz window in a nitrogen-

filled container. The thickness of the active layers in the photovoltaic devices was measured on a Veeco Dektak 150 profilometer.

The spectrally IQE was determined by optical modeling of the entire layer stack using the wavelength dependent refractive index (n) and extinction coefficient (k).[52] Calculations of the optical electric field were performed with Setfos 3 (Fluxim AG, Switzerland). The averaged IQE was determined by convolution of the solar spectrum with the EQE of the solar cell and the absorbed photon flux.

4.2. 3,6-Bis(5′-bromo-4′-dodecyl-[2,2′-bithiophen]-5-yl)-2,5-bis(2-hexyldecyl)pyrrolo[3,4-c]pyrrole-1,4(2H,5H)-dione (3). To a degassed solution of 3,6-bis(5-bromo-2-thienyl)-2,5-dihydro-2,5-di(2′-hexyldecyl)-pyrrolo[3,4c]pyrrolo-1,4-dione (**1**) (0.907 g, 1 mmol), 2-(4-dodecylthiophen-2-yl)-4,4,5,5-tetramethyl-1,3,2-dioxaborolane (0.833 g, 2.2 mmol), 2 M K_2CO_3 solution in H_2O (1.5 mL), toluene (15 mL), Aliquat 336 (0.5 mL), tetrakis(triphenylphosphine)-palladium(0) (58 mg, 0.05 mmol) were added. The mixture was stirred at 115 °C for 24 h. The resulting mixture was cooled to room temperature after which it was poured out in chloroform, washed by water and brine, and dried by evaporation. The crude product was dissolved into small amount of chloroform and precipitated into methanol to afford **2** (yield 1.062 g) which was directly used for next step. To a solution of **2** (1.062 g, 0.85 mmol) in chloroform (30 mL) at 0 °C, *N*-bromosuccinimide (303 mg, 1.70 mmol) was added in portions in 20 min, and the reaction mixture was stirred in another 30 min at 0 °C. After this the mixture was poured out in chloroform, washed with water and brine, and evaporated. The resulting solid was subjected to column chromatography (silica, eluent heptane/CH_2Cl_2, 75%/25%) to yield 1.077 g (0.765 mmol, 90%) of a black solid. ^{1}H NMR δ (ppm): 8.82 (d, 2H), 7.17 (d, 2H), 6.97 (s, 2H), 3.99 (d, 4H), 2.55 (t, 4H), 1.92 (m, 2H), 1.59 (m, 4H), 1.30 (m, 84H), 0.86 (m, 18H). ^{13}C NMR δ (ppm): 161.58, 143.55, 141.84, 139.27, 136.41, 135.66, 128.22, 125.68, 124.47, 109.96, 108.40, 46.26, 37.94, 31.94, 29.74, 29.70, 29.68, 29.66, 29.61, 29.60, 14.13, 14. MS (MALDI): calcd, 1407.88; found, 1406.64 (M^+).

4.3. PDPP4TN. To a degassed solution of monomer **3** (56.93 mg, 0.040 mmol), 2,2′-(2,6-naphthalenediyl)bis[4,4,5,5-tetramethyl-1,3,2-dioxaborolane (**4**) (15.37 mg, 0.040 mmol) in H_2O (0.5 mL) and THF (3 mL) containing 2 M K_3PO_4, tris(dibenzylideneacetone)-dipalladium(0) (1.48 mg, 1.6 μmol) and tri*tert*-butylphosphonium tetrafluoroborate (0.94 mg, 3.2 μmol) were added. The mixture was stirred at 80 °C for 24 h, after which it was precipitated in methanol. The solids were filtered off, redissolved in chloroform (50 mL), and refluxed with 28% NH_3 solution in water (50 mL) for 1 h. The layers were separated, and the organic layer was stirred with EDTA (100 mg) for 2 h, after which water (100 mL) was added, and the liquids were stirred for 1 h. The layers were separated, and the organic layer was reduced in volume by evaporating most of the chloroform. The polymer was precipitated in acetone and filtered through a Soxhlet thimble. The polymer was extracted with acetone, hexane, and chloroform. The chloroform fraction was evaporated, and the polymer was precipitated in acetone. The polymer was collected by filtering over a 0.45 μm PTFE membrane filter and dried in a vacuum oven to yield **PDPP4TN** (45.3 mg, 82.4%) as a dark powder. ^{1}H NMR δ (ppm): 8.91 (b, 4H), 7.62 (b, 4H), 7.22 (b, 2H), 6.94 (b, 2H), 4.06 (b, 4H), 2.75 (b, 4H), 1.89 (b, 2H), 1.59 (b, 4H), 1.30 (b, 84H), 0.86 (b, 18H). GPC (*o*-DCB, 80 °C): M_n = 12.1 kg mol^{-1}, PDI = 3.11.

4.4. PDPP4TP. Same procedure as for **PDPP4TN** was used, but now **3** (88.01 mg, 0.0625 mmol) and 1,4-di-(4,4,5,5-tetramethyl-1,3-dioxaborolane)benzene (**5**) (20.631 mg, 0.0625 mmol) were used as the monomers. Yield: 56 mg (67.7%). ^{1}H NMR δ (ppm): 8.91 (b, 4H), 7.52 (b, 2H), 7.22 (b, 2H), 6.89 (b, 2H), 4.07 (b, 4H), 2.71 (b, 4H), 1.89 (b, 2H), 1.59 (b, 4H), 1.30 (b, 84H), 0.86 (b, 18H). GPC (*o*-DCB, 80 °C): M_n = 32.4 kg mol^{-1}, PDI = 2.69.

4.5. PDPP4TBDT. To a degassed solution of monomer **3** (0.1 g, 0.071 mmol), 2,6-bis(trimethyltin)-4,8-bis(5-hexylthiophene-2-yl)-benzo[1,2-*b*:4,5-b′]dithiophene (**6**) (60.27 mg, 0.071 mmol) in toluene (3 mL) and DMF (0.6 mL), tris(dibenzylideneacetone)-dipalladium(0) (2.6 mg, 2.84 μmol), and triphenylphosphine (1.49 mg, 5.68 μmol) were added. The mixture was stirred at 115 °C for 24 h, after which it was precipitated in methanol. The solids were filtered off, redissolved in chloroform (50 mL), and refluxed with 28% NH_3 solution in water (50 mL) for 1 h. The layers were separated, and the organic layer was stirred with EDTA (100 mg) for 2 h, after which water (100 mL) was added, and the liquids were stirred for 1 h. The layers were separated, and the organic layer was reduced in volume by evaporating most of the chloroform. The polymer was precipitated in acetone and filter through a Soxhlet thimble. The polymer was extracted with acetone, hexane, and chloroform. The chloroform fraction was evaporated, and the polymer was precipitated in acetone. The polymer was collected by filtering over a 0.45 μm PTFE membrane filter and dried in a vacuum oven to yield **PDPP4TBDT** (105 mg, 83.6%) as a dark powder. ^{1}H NMR δ (ppm): 8.88 (b, 4H), 7.50 (b, 2H), 7.00 (b, 8H), 4.05 (b, 4H), 2.97 (b, 8H), 1.89 (b, 2H), 1.59 (b, 8H), 1.30 (b, 100H), 0.86 (b, 24H). GPC (*o*-DCB, 80 °C): M_n = 41.8 kg mol^{-1}, PDI = 3.03.

4.6. PDPP4TTT. Same procedure as for **PDPP4TBDT** was used, but now **3** (72.65 mg, 0.0516 mmol) and 2,5-bis(trimethylstannyl)-thieno[3,2-b]thiophene (**7**) (24.04 mg, 0.0516 mmol) were used as the monomers. Yield: 35 mg (48.9%). The low yield originated from the insoluble high molecular weight part. ^{1}H NMR δ (ppm): 8.89 (b, 4H), 7.00 (b, 4H), 4.05 (b, 4H), 2.78 (b, 4H), 1.90 (b, 2H), 1.59 (b, 4H), 1.30 (b, 84H), 0.86 (b, 18H). GPC (*o*-DCB, 80 °C): M_n = 22.8 kg mol^{-1}, PDI = 3.0.

4.7. PDPP6T. Same procedure as for **PDPP4TBDT** was used, but now **3** (63.43 mg, 0.0451 mmol) and 5,5′-bis(trimethylstannyl)-2,2′-bithiophene (**8**) (22.16 mg, 0.0451 mmol) were used as the monomers. Yield: 52 mg (81.6%). ^{1}H NMR δ (ppm): 8.90 (b, 4H), 7.00 (b, 6H), 4.05 (b, 4H), 2.70 (b, 4H), 1.95 (b, 2H), 1.59 (b, 4H), 1.30 (b, 84H), 0.86 (b, 18H). GPC (*o*-DCB, 80 °C): M_n = 37.9 kg mol^{-1}, PDI = 2.95.

4.8. PDPP5T. Same procedure as for **PDPP4TBDT** was used, but now **3** (57.59 mg, 0.0409 mmol) and 5,5′-bis(trimethylstannyl)-thiophene (**9**) (16.76 mg, 0.0409 mmol) were used as the monomers. Yield: 48 mg (88.2%). ^{1}H NMR δ (ppm): 8.92 (b, 4H), 7.01 (b, 4H), 4.06 (b, 4H), 2.74 (b, 4H), 1.91 (b, 2H), 1.59 (b, 4H), 1.30 (b, 84H), 0.86 (b, 18H). GPC (*o*-DCB, 80 °C): M_n = 36.8 kg mol^{-1}, PDI = 3.03.

■ ASSOCIATED CONTENT

Supporting Information

GPC traces, cyclic voltammetry data, AFM images, optical constants, and molecular weight dependence of solar cell performance on molecular weight for PDPP4TP. This material is available free of charge via the Internet at http://pubs.acs.org.

■ AUTHOR INFORMATION

Corresponding Author

r.a.j.janssen@tue.nl

Notes

The authors declare no competing financial interest.

■ ACKNOWLEDGMENTS

This work was performed in the framework of the "Largecells" project that received funding from the European Commission's Seventh Framework Programme (FP7/2007-2013) under grant agreement no. 261936. The research was further supported by the "Europees Fonds voor Regionale Ontwikkeling" (EFRO) in the Interreg IV-A project Organext.

■ REFERENCES

(1) Li, G.; Zhu, R.; Yang, Y. *Nat. Photonics* **2012**, *6*, 153−161.
(2) Li, Y. F. *Acc. Chem. Res.* **2012**, *45*, 723−733.
(3) Cheng, Y. J.; Yang, S. H.; Hsu, C. S. *Chem. Rev.* **2009**, *109*, 5868−5923.
(4) Duan, C.; Huang, F.; Cao, Y. *J. Mater. Chem.* **2012**, *22*, 10416−10434.

(5) Boudreault, P. T.; Najari, A.; Leclerc, M. *Chem. Mater.* **2011**, *23*, 456−469.
(6) Huo, L.; Zhang, S.; Guo, X.; Xu, F.; Li, L.; Hou, J. *Angew. Chem., Int. Ed.* **2011**, *50*, 9697−9702.
(7) Amb, C. M.; Chen, S.; Graham, K. R.; Subbiah, J.; Small, C. E.; So, F.; Reynolds, J. R. *J. Am. Chem. Soc.* **2011**, *133*, 10062−10065.
(8) Zhao, G.; He, Y.; Li, Y. *Adv. Mater.* **2010**, *22*, 4355−4358.
(9) Liang, Y.; Xu, Z.; Xia, J.; Tsai, S.-T.; Wu, Y.; Li, G.; Ray, C.; Yu, L. *Adv. Mater.* **2010**, *22*, E135−E138.
(10) Chen, H.-Y.; Hou, J.; Zhang, S.; Liang, Y.; Yang, G.; Yang, Y.; Yu, L.; Wu, Y.; Li, G. *Nat. Photonics* **2009**, *3*, 649−653.
(11) Piliego, C.; Holcombe, T. W.; Douglas, J. D.; Woo, C. H.; Beaujuge, P. M.; Fréchet, J. M. J. *J. Am. Chem. Soc.* **2010**, *132*, 7595−7597.
(12) Wang, E.; Ma, Z.; Zhang, Z.; Vandewal, K.; Henriksson, P.; Inganäs, O.; Zhang, F.; Andersson, M. R. *J. Am. Chem. Soc.* **2011**, *133*, 14244−14247.
(13) He, Z.; Zhong, C.; Huang, X.; Wong, W. Y.; Wu, H.; Chen, L.; Su, S.; Cao, Y . *Adv. Mater.* **2011**, *23*, 4636−4643.
(14) Small, C. E.; Chen, S.; Subbiah, J.; Amb, C. M.; Tsang, S.-W.; Lai, T.-H.; Reynolds, J. R.; So, F. *Nat. Photonics* **2012**, *6*, 115−120.
(15) Yiu, A. T.; Beaujuge, P. M.; Lee, O. P.; Woo, C. H.; Toney, M. F.; Fréchet, J. M. J. *J. Am. Chem. Soc.* **2012**, *134*, 2180−2185.
(16) Chu, T.-Y.; Lu, J.; Beaupre, S.; Zhang, Y.; Pouliot, J.-R.; Zhou, J.; Najari, A.; Leclerc, M.; Tao, Y. *Adv. Funct. Mater.* **2012**, *22*, 2345−2351.
(17) Huang, F.; Guo, X.; Liu, F.; Huo, L. J.; Chen, Y. N.; Russell, T. P.; Han, C. C.; Li, Y. F.; Hou, J. H. *Adv. Mater.* **2012**, *24*, 3383−3389.
(18) Gevaerts, V. S.; Furlan, A.; Wienk, M. M.; Turbiez, M.; Janssen, R. A. J. *Adv. Mater.* **2012**, *24*, 2130−2134.
(19) Dou, L. T.; You, J. B.; Yang, J.; Chen, C. C.; He, Y. J.; Murase, S.; Moriarty, T.; Emery, K.; Li, G.; Yang, Y. *Nat. Photonics* **2012**, *6*, 180−185.
(20) Dennler, G.; Scharber, M. C.; Ameri, T.; Denk, P.; Forberich, K.; Waldauf, C.; Brabec, C. J. *Adv. Mater.* **2008**, *20*, 579−583.
(21) Blom, P. W. M.; Mihailetchi, V. D.; Koster, L. J. A.; Markov, D. E. *Adv. Mater.* **2007**, *19*, 1551−1566.
(22) Bürgi, L.; Turbiez, M.; Pfeiffer, R.; Bienewald, F.; Kirner, H. J.; Winnewisser, C. *Adv. Mater.* **2008**, *20*, 2217−2224.
(23) Wienk, M. M.; Turbiez, M.; Gilot, J.; Janssen, R. A. J. *Adv. Mater.* **2008**, *20*, 2556−2560.
(24) Bijleveld, J. C.; Zoombelt, A. P.; Mathijssen, S. G. J.; Wienk, M. M.; Turbiez, M.; de Leeuw, D. M.; Janssen, R. A. J. *J. Am. Chem. Soc.* **2009**, *131*, 16616−16617.
(25) Bronstein, H.; Chen, Z.; Ashraf, R. S.; Zhang, W.; Du, J.; Durrant, J. R.; Tuladhar, P. S.; Song, K.; Watkins, S. E.; Geerts, Y.; Wienk, M. M.; Janssen, R. A. J.; Anthopoulos, T.; Sirringhaus, H.; Heeney, M.; McCulloch, I. *J. Am. Chem. Soc.* **2011**, *133*, 3272−3275.
(26) Park, S. H.; Roy, A.; Beaupre, S.; Cho, S.; Coates, N.; Moon, J. S.; Moses, D.; Leclerc, M.; Lee, K.; Heeger, A. J. *Nat. Photonics* **2009**, *3*, 297−302.
(27) Bijleveld, J. C.; Gevaerts, V. S.; Di Nuzzo, D.; Turbiez, M.; Mathijssen, S. G. J.; de Leeuw, D. M.; Wienk, M. M.; Janssen, R. A. J. *Adv. Mater.* **2010**, *22*, E242−E246.
(28) Zhang, F. L.; Bijleveld, J.; Perzon, E.; Tvingstedt, K.; Barrau, S.; Inganas, O.; Andersson, M. R. *J. Mater. Chem.* **2008**, *18*, 5468−5474.
(29) Bijleveld, J. C.; Verstrijden, R. A. M.; Wienk, M. M.; Janssen, R. A. J. *J. Mater. Chem.* **2011**, *21*, 9224−9231.
(30) Zoombelt, A. P.; Mathijssen, S. G. J.; Turbiez, M. G. R.; Wienk, M. M.; Janssen, R. A. J. *J. Mater. Chem.* **2010**, *20*, 2240−2246.
(31) Zoombelt, A. P.; Fonrodona, M.; Wienk, M. M.; Sieval, A. B.; Hummelen, J. C.; Janssen, R. A. J. *Org. Lett.* **2009**, *11*, 903−906.
(32) Ohkita, H.; Cook, S.; Astuti, Y.; Duffy, W.; Tierney, S.; Zhang, W.; Heeney, M.; McCulloch, I.; Nelson, J.; Bradley, D. D. C.; Durrant, J. R. *J. Am. Chem. Soc.* **2008**, *130*, 3030−3042.
(33) Veldman, D.; Meskers, S. C. J.; Janssen, R. A. J. *Adv. Funct. Mater.* **2009**, *19*, 1939−1948.
(34) Vandewal, K.; Tvingstedt, K.; Gadisa, A.; Inganäs, O.; Manca, J. V. *Nat. Mater.* **2009**, *8*, 904−909.
(35) Bakulin, A. A.; Rao, A.; Pavelyev, V. G.; van Loosdrecht, P. H. M.; Pshenichnikov, M. S.; Niedzialek, D.; Cornil, J.; Beljonne, D.; Friend, R. H. *Science* **2012**, *335*, 1340−1344.
(36) Vandewal, K.; Ma, Z.; Bergqvist, J.; Tang, Z.; Wang, E.; Henriksson, P.; Tvingstedt, K.; Andersson, M. R.; Zhang, F.; Inganäs, O. *Adv. Funct. Mater.* **2012**, DOI: 10.1002/adfm.201200608.
(37) van Eersel, H.; Janssen, R. A. J.; Kemerink, M. *Adv. Funct. Mater.* **2012**, *22*, 2700−2708.
(38) van der Hofstad, T. G. J.; Di Nuzzo, D.; van den Berg, M.; Janssen, R. A. J.; Meskers, S. C. J. *Adv. Energy Mater.* **2012**, DOI: 10.1002/aenm.201200030.
(39) Brabec, C. J.; Winder, C.; Sariciftci, N. S.; Hummelen, J. C.; Dhanabalan, A.; van Hal, P. A.; Janssen, R. A. J. *Adv. Funct. Mater.* **2002**, *12*, 709−712.
(40) Koster, L. J. A.; Mihailetchi, V. D.; Blom, P. W. M. *Appl. Phys. Lett.* **2006**, *88*, 093511/1−3.
(41) Wienk, M. M.; Kroon, J. M.; Verhees, W. J. H.; Knol, J.; Hummelen, J. C.; van Hal, P. A.; Janssen, R. A. J. *Angew. Chem., Int. Ed.* **2003**, *42*, 3371−3375.
(42) Coffin, R. C.; Peet, J.; Rogers, J.; Bazan, G. C. *Nat. Chem.* **2009**, *1*, 657−661.
(43) Yiu, A. T.; Beaujuge, P. M.; Lee, O. P.; Woo, C. H.; Toney, M. F.; J. Fréchet, J. M. *J. Am. Chem. Soc.* **2012**, *134*, 2180−2185.
(44) Lee, J.; Vandewal, K.; Yost, S. R.; Bahlke, M. E.; Goris, L.; Baldo, M. A.; Manca, J. V.; Voorhis, T. V. *J. Am. Chem. Soc.* **2010**, *132*, 11878−11880.
(45) Drori, T.; Holt, J.; Vardeny, Z. V. *Phys. Rev. B* **2010**, *82*, 075207/1−8.
(46) Street, R. A.; Song, K. W.; Northrup, J. E.; Cowan, S. *Phys. Rev. B* **2011**, *83*, 165207/1−13.
(47) Kong, H.; Chung, D. S.; Kang, I. N.; Park, J. H.; Park, M. J.; Jung, I. H.; Park, C. E.; Shim, H. K. *J. Mater. Chem.* **2009**, *19*, 3490−3499.
(48) Sonar, P.; Singh, S. P.; Li, Y. N.; Ooi, Z. E.; Ha, T. J.; Wong, I.; Soh, M. S.; Dodabalapur, A. *Energy Environ. Sci.* **2011**, *4*, 2288−2296.
(49) Huo, L. J.; Zhang, S. Q.; Guo, X.; Xu, F.; Li, Y. F.; Hou, J. H. *Angew. Chem., Int. Ed.* **2011**, *50*, 9697−9702.
(50) Subramaniyan, S.; Xin, H.; Kim, F. S.; Jenekhe, S. A. *Macromolecules* **2011**, *44*, 6245−6248.
(51) Cho, C. H.; Kang, H.; Kang, T. E.; Cho, H. H.; Yoon, S. C.; Jeon, M. K.; Kim, B. J. *Chem. Commun.* **2011**, *47*, 3577−3579.
(52) Gilot, J.; Wienk, M. M.; Janssen, R. A. J. *Adv. Mater.* **2010**, *22*, E67−E71.